# On the similarity between discrete harmonic wavelet and discrete orthonormal S transform

X.Z. Cui
*Assistant Professor, School of Civil and Environmental Engineering, Harbin Institute of Technology, Shenzhen, China. Email: cuixizhong@hit.edu.cn*

Y.X. Liu
*Ph.D. Candidate, Department of Civil and Environmental Engineering, University of Western Ontario, London, Canada. Email: yliu3863@uwo.ca*

W.X. Zhou
*Professor, Department of Civil and Environmental Engineering, University of Western Ontario, London, Canada. Email: wzhou@eng.uwo.ca*

H.P. Hong
*Professor, Department of Civil and Environmental Engineering, University of Western Ontario, London, Canada. Email: hhong@uwo.ca*

ABSTRACT: Two efficient transforms: discrete harmonic wavelet transform (DHWT) and discrete orthonormal S transform (DOST) were developed in the literature. They can be used to analyze, model, and simulate nonstationary signals. Both transforms are efficient and have been used to represent seismic ground motions and wind speeds of high-intensity wind events. The efficiency arises from the fact that they are non-redundant transforms which is similar to Fourier transform but can cope with temporal varying characteristics. DOST originated from the summation of Fourier representation over a frequency band and considers phase shift such that the basis functions are absolutely referenced. DHWT originated from the wavelet concept (i.e., continuous harmonic wavelets). Its basic function is also obtained by considering a frequency band. However, the phase of the basis function is not absolutely referenced. It seems that a detailed discussion of their similarity is never provided in the literature. In fact, papers using DHWT for engineering applications rarely mention DOST and vice versa. In the present study, we provide a detailed comparison of these two transforms in terms of the mathematical derivation of their basis functions, their computer implementation, and their characteristics, including edge effects. In addition, we show their potential use in simulating nonstationary processes. To minimize the edge effects by using DHWT and DOST as well as their variants, we suggest an iterative correction algorithm, which is illustrated by simulating nonstationary processes.

## 1. INTRODUCTION

Signal processing methods are widely adopted in the analysis, modelling, and simulation of signals, such as seismic ground motion records and wind speed records. In practical engineering, the signals to be analyzed always exhibit significant nonstationary characteristics. To obtain the nonstationary features of the signals, continuous wavelet transform (CWT) (Daubechies 1992) and S-transform (ST) (Stockwell et al 1996) are widely used and they could provide representations in time-scale space and time-frequency space, respectively. However, both CWT and ST are highly redundant transforms. They demand a high computational effort for the analysis of long-duration signals or large images and can be inefficient. If the wavelet transform is considered, this inefficiency could be overcome by using the discrete wavelet transform, which is a transform with a low degree of redundancy or non-redundant transform. A discrete wavelet transform, such as the discrete harmonic wavelet transform (DHWT) (Newland 1994), provides the phase information. DHWT was developed from the wavelet concept (i.e., continuous harmonic wavelets). Its basis function is obtained by wrapping the Fourier representation over a frequency band. However, the phase of the basis function is not absolutely referenced.

If the time-frequency type of transform, such as the S-transform or the discrete orthonormal S-transform (DOST) (Stockwell 2007) is considered, absolute-reference phase information (i.e., similar to the Fourier transform) is retained. The basis functions of DOST are derived from the summation of Fourier representation over a frequency band but with phase shifts. DOST is a non-redundant transform.

Both DHWT and DOST are efficient and have been used to represent and simulate seismic ground motions and wind speeds of high-intensity wind events (Spanos and Failla 2004; Cui and Hong 2020; Hong et al. 2021). However, it seems that a detailed discussion of their similarity and difference is not available in the literature. In fact, papers using DHWT for engineering applications rarely mention DOST and vice versa.

In the present study, we provide a detailed comparison of these two transforms in terms of the mathematical derivation of their basis functions, their computational implementation, and their characteristics, including edge effects. In addition, we show their potential use in simulating nonstationary processes. To minimize the edge effects by using DHWT and DOST, we suggest an iterative correction procedure, which is illustrated by simulating nonstationary processes.

## 2. BRIEF REVIEW OF DHWT AND DOST

### *2.1. Mother wavelet for HWT and DHWT pair*

The wavelet transform for a continuous signal $x(t)$ is defined as (Percival and Walden 2000),

$$x_{\mathcal{W}}(s,\tau) = \left(1/\sqrt{|s|}\right)\int_{-\infty}^{\infty} x(t)\psi^*\left(\left(t-\tau\right)/s\right)dt \quad (1)$$

where $x_{\mathcal{W}}(s,\tau)$ is the wavelet coefficient; $\psi(\cdot)$ is the mother wavelet; $s$ and $\tau$ are the scale and translation parameters; * is the complex conjugate.

For the harmonic wavelet with selected parameters, $\psi(\cdot)$, denoted as $\psi_H(t)$, can be written as (Newland 1993),

$$\psi_H(t) = (e^{i4\pi t} - e^{i2\pi t})/(i2\pi t) \quad (2)$$

and the Fourier transform of $\psi_H(t)$, denoted as $\hat{\psi}_H(f)$, is

$$\hat{\psi}_H(f) = \begin{cases} 1, & 1 \le f < 2 \\ 0, & \text{otherwise} \end{cases} \quad (3)$$

Consider that $x(t)$ could be represented as an $N$-point real-valued discrete signal $x(t_k)$ with $t_k = (k\text{-}1)\Delta t$, where $\Delta t$ is the time increment and $k$ = 1, 2, … $N$. By partitioning the transform domain, selecting the scale $s = 2^{-b}N\Delta t$ and the time location $\tau = (2^{-b}N\Delta_t)q$, and using a proper normalization constant, one obtains the basic function for DHWT, $\psi_{DH}(t_k;b,q)$, at time $t_k$, given by (Newland 1994),

$$\psi_{DH}(t_k;b,q) = (2^b)^{1/2}\psi_H(2^b k/N - q) \quad (4)$$

where $b$ is known as the level number (i.e., selected based on the octave sampling rule which will be elaborated on in the next section) and $q$ is the time localization index.

The DHWT coefficients of $x(t_k)$, $x_{DH}(b,q)$, for $b = 0,...,\nu-2$, and $q = 0,...,2^b-1$ can be calculated using (Newland 1993),

$$x_{DH}(b,q) = \frac{1}{N}\sum_{k=0}^{N-1} x(t_k)\psi^*_{DH}(t_k;b,q) \quad (5)$$

where the number of decomposition levels $\nu$ is determined by the sample size $N = 2^\nu$. $x(t_k)$ can be reconstructed using (Newland 1993; Spanos et al. 2005),

$$x(t_k) = 2\,\mathrm{Re}\left[\sum_{b=0}^{\nu-2}\sum_{q=0}^{2^b-1} x_{DH}(b,q)\psi_{DH}(t_k;b,q)\right] \quad (6)$$

However, the use of Eq. (6) for a signal with finite duration does not ensure the perfect reconstruction. This will be elaborated on in the following sections.

### *2.2. Basis functions of DOST, and transform pair*

The basis function used in DOST is derived by taking linear combinations of the original Fourier basis functions in band-limited subspaces and applying the appropriate frequency and phase shift (Stockwell 2007), which results in,

$$D_{[\beta]}(t_k; p, q) = \frac{1}{\sqrt{\beta}} \sum_{r=p-\beta/2}^{r=p+\beta/2-1} \left[ \exp\left(i2\pi\left(k\Delta_t\right)\left(r\Delta_f\right)\right) \times \exp\left(-i2\pi\left(\frac{q}{\beta}T\right)\left(r\Delta_f\right)\right) \times \exp\left(-i\left(\frac{q}{\beta}T\right)\left(\frac{\pi\beta}{T}\right)\right) \right] \tag{7}$$

where $p$ and $q$ are the indices for the center of the frequency band, $p\Delta_f$, and time localization $q\Delta_t$, respectively. The width of each frequency band, $\beta\Delta_f$, is indexed by $\beta$. $\Delta_f$ is the frequency increment, which is the same as that defined in the discrete Fourier transform and equals $1/(N\Delta_t)$. Through algebraic manipulation, Eq. (7) is simplified to,

$$D_{[\beta]}(t_k; p, q) = ie^{-i\pi q} \left[ e^{i2\pi(\frac{k}{N}-\frac{q}{\beta})(p-\frac{\beta}{2}-\frac{1}{2})} - e^{i2\pi(\frac{k}{N}-\frac{q}{\beta})(p+\frac{\beta}{2}-\frac{1}{2})} \right] / \left\{ 2\sqrt{\beta}\sin[\pi(k/N - q/\beta)] \right\} \tag{8}$$

For $D_{[\beta]}(t_k; p, q)$ to be orthonormal basis functions, Stockwell (2007) suggested that $q = 0, 1, \ldots, \beta - 1$, and $p$ and $\beta$ can be selected by using octave sampling. This leads to $(p; q; \beta)|_{m=0} = (0;0;1)$, $(p; q; \beta)|_{m=1} = (1;0;1)$, and $(p;q;\beta)\big|_{m=2,\ldots,\log_2(N)-1} = (2^{m-1}+2^{m-2}; 0,\ldots,2^{m-1}-1; 2^{m-1})$, where $m$ is the octave number which is similar to the level number $b$ in Eq. (4) for DHWT. For the same time index, the vector of the basis functions for the positive frequency band $p$ is conjugate symmetric to the corresponding vector of the basis functions for the negative frequency band $-p$ (Wang and Orchard 2009).

The DOST coefficients of $x(t_k)$ are calculated using,

$$x_{\mathfrak{D}}(p, q; \beta) = \sum_{k=0}^{N-1} x(t_k) D_{[\beta]}(t_k; p, q) \tag{9}$$

The signal $x(t_k)$ can be reconstructed using,

$$x(t_k) = \sum_{\text{all } p,q} x_{\mathfrak{D}}(p, q; \beta) D^{*}_{[\beta]}(t_k; p, q) \tag{10}$$

## 3. COMPARISON BETWEEN DOST AND DHWT

In the following, we discuss the similarities and differences between DOST and DHWT in three aspects: 1) derivation and properties of basis functions; 2) computational implementation; 3) representation in time-frequency or time-scale space. Also, the definitions of power spectral density (PSD) based on DOST and DHWT are elaborated. To aid the discussion and comparison, a seismic ground motion record shown in Figure 1a is used as the seed record.

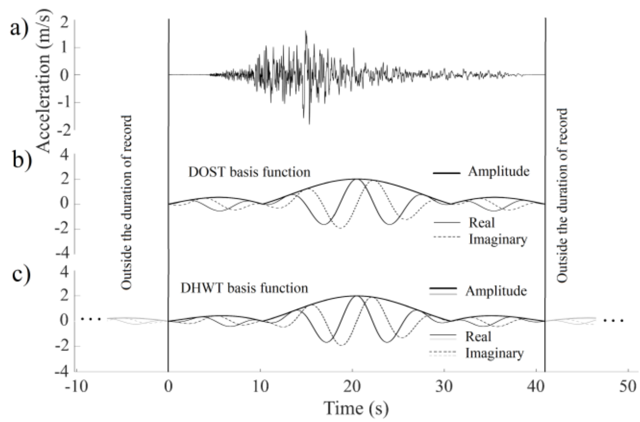


*Figure 1: a) A seed record for the comparison; b) a basis function for DOST ((p; q; β)=(6,2,4)); c) a basis function for DHWT ((b, q)=(2,2)). (The part outside the duration of the considered record is marked as grey)*

### *3.1. Derivation and properties of basis functions*

There are mainly two differences between Eqs. (4) and (7), which are described in the following.

1) While the DOST basis functions are derived based on discrete Fourier transform (DFT), those for DHWT are obtained by selecting the

values of the continuous harmonic wavelet function at discrete values in scale and time location. The latter can be viewed as an approximation to the continuous Fourier transform (CFT).

CFT is a transform for a continuous function of time, while the DFT is a transform designed for the discrete time series with finite length (Bracewell 1986). A basis function for DOST with ($p$; $q$; β) = (6; 2; 4) and a basis function for DHWT with ($b$, $q$) = (2; 2) are shown in Figures 1b and 1c, respectively. The selections of the values for $p$ and $b$ correspond to the same frequency band in octave sampling. The figure shows that the two basis functions depict a similar shape. While the basis function for DOST is defined only for the time interval shown, the DHWT basis function is defined over the real axis. Moreover, the values of the basis functions shown in Figures 1b and 1c are not identical, partly because the required normalization for the basis functions is defined within their corresponding intervals. This has implications for signal reconstruction and energy preservation for DHWT in dealing with a digitized signal of finite duration.

Also, the orthonormal conditions for the basis function in DOST and DHWT are,

$$\frac{1}{N}\sum_{k=1}^{N} D_{[\beta_1]}(t_k; p_1, q_1) D^*_{[\beta_2]}(t_k; p_2, q_2) = \begin{cases} 0 & \text{for } (p_1, q_1) \neq (p_2, q_2) \\ 1 & \text{for } (p_1, q_1) = (p_2, q_2) \end{cases} \tag{11}$$

and,

$$\lim_{N->\infty} \frac{1}{N} \sum_{k=-N/2+(N/2^b)q}^{+N/2+(N/2^b)q} \psi_{DH}(t_k; b_1, q_1) \psi^*_{DH}(t_k; b_2, q_2) = \begin{cases} 0 & \text{for } (b_1, q_1) \neq (b_2, q_2) \\ 1 & \text{for } (b_1, q_1) = (b_2, q_2) \end{cases} \tag{12}$$

The orthonormal condition for Eq. (11) is defined for the duration of the considered signal while such a condition for Eq. (12) is defined over the entire real axis. The DHWT basis functions are not orthonormal if only a finite duration corresponding to the duration of the considered signal is considered. Therefore, the consideration of coefficients for the frequencies within the Nyquist frequency cannot result in energy preservation and is associated with energy leakage. Consequently, the direct use of DHWT (i.e., Eqs. (5) and (6)) for a signal $x(t_k)$ of finite duration does not ensure its perfect reconstruction.

To illustrate this, we first apply Eq. (5) to the signal shown in Figure 1a to calculate $x_{DH}(b,q)$. We then use the obtained $x_{DH}(b,q)$ and Eq. (6) to reconstruct the record. Both the original and reconstructed records are shown in Figure 2, illustrating their differences. In this case, the total energy of the original record and of the reconstructed record are 2.8633 $m^2/s^3$ and 2.8530 $m^2/s^3$, respectively. Note that a perfect reconstruction is achieved if the DOST pair (i.e., Eqs. (9) and (10)) are employed.

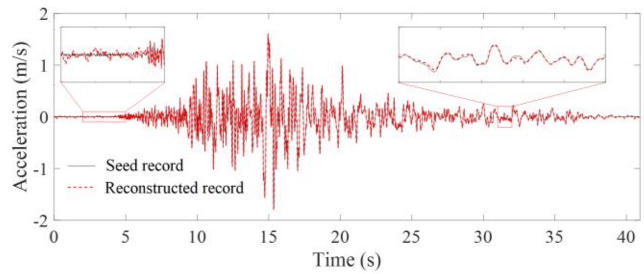


*Figure 2: Comparison between the reconstructed signal using Eqs. (6) and (7) by considering the signal shown in Figure 1a.*

2) The phase of the DOST coefficients is absolutely referenced while that of DHWT is locally referenced (i.e., referenced with the considered time localization).

This can be explained by noting that an additional phase shift is considered in Eq. (7) to ensure the phase of the DOST basis functions is absolutely referenced. The use of the absolutely referenced phase can be advantageous since its interpretation is consistent with that of the Fourier transform. It allows building the relationship to the instantaneous frequency and bringing meanings to the phase of the complex coefficients (Stockwell 2007).

### *3.2. Computational implementation*

The use of FFT to enhance the computational efficiency of using DOST is extensively elaborated in Stockwell (2007) and, Wang and Orchard (2009). Consider the record shown in Figure 1a which has 4096 discrete values, denoted as $a_1$, $a_2$, …, $a_{4096}$. Figure 3 shows the algorithm using FFT for DOST for the considered record.

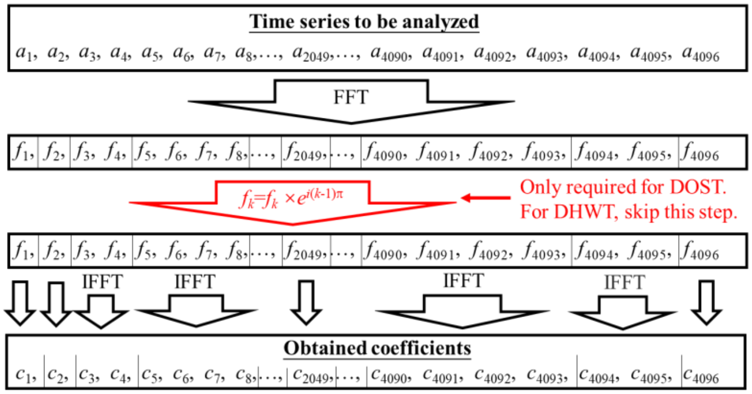


*Figure 3: Algorithm of numerical implementation for DOST and DHWT by using FFT.*

As discussed above, the use of DHWT that is defined in Eqs. (5) and (6) cannot perfectly reconstruct the analyzed signal and distorts the total energy. In practical applications, DHWT is performed in the discrete frequency domain instead of the time domain (i.e., Eqs. (5) and (6)); which facilitates the use of FFT for the numerical evaluation. A detailed explanation and computer implementation by using FFT to carry out DHWT are given by Newland (1993). In fact, such an implementation is the same as that for DOST shown in Figure 3, except that the marked phase shift in Figure 3 is not included for DHWT. Note that the algorithm shown in Figure 3 is for the analysis of real-valued time series, it does not apply directly to the complex-valued signal. Unlike the DHWT pair in the time domain, the implementation of DHWT as shown in Figure 3 can perfectly reconstruct the signal.

In conclusion, although the DOST and DHWT are different in their derivations and properties of basis functions, their computational implementations are almost identical by using FFT. The main difference is that DOST adopted an additional phase shift to ensure the phase is absolutely referenced. The theoretical derivation and implementation for DOST are consistent, while strictly speaking, there is an inconsistency between the theoretical derivation of DHWT and its computer implementation, although such inconsistency is likely to be inconsequential for some practical applications.

### *3.3. Representation in time-frequency space or time-scale space*

The discussion in this section is focused on the partition of the transform domain for DOST and DHWT.

The partition of the transform domain for DHWT by considering the octave (dyadic) sampling is shown in Figure 4a. This transform domain is in the time-scale space. To obtain the representation in the time-frequency space, an exact or approximate relationship between the scale $s$ and the frequency $f$, which is can be stated as $f = 3/2s$ (Hz), is required. Using this relationship, the representation of DHWT in the time-scale space can be mapped to the time-frequency space as shown in Figure 4b. Because both DOST and DHWT adopted the octave (or dyadic) sampling rule, the representation in time-frequency space shown in Figure 4b is also applicable to DOST. That means although the obtained coefficients from DOST and DHWT are different, the mapping between the coefficients and the partitioned blocks in time-frequency space is the same. It must be emphasized that the discussions in the following are based on the computer implementation of DHWT rather than on its theoretical formulation and definition.

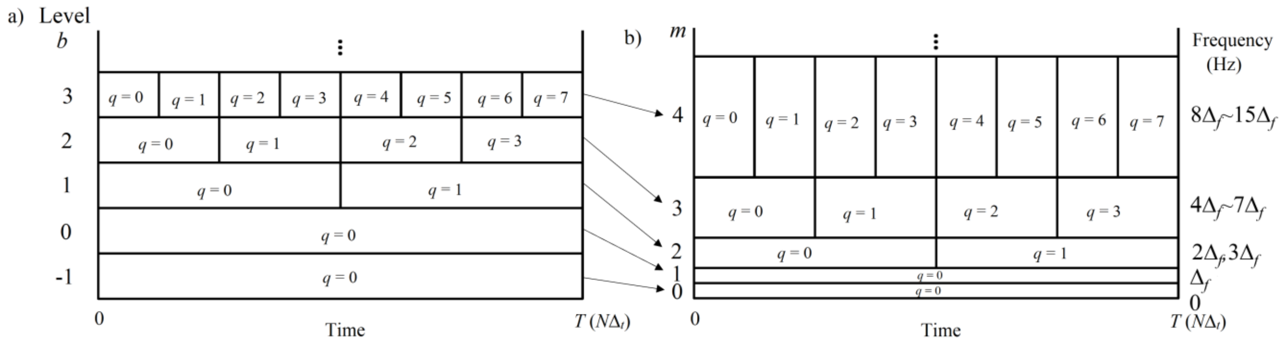


*Figure 4: Partition of a) time-scale domain for DHWT; b) time-frequency domain for both DOST and DHWT.*

### *3.4. PSD definition*

The concept of energy distribution is important for the simulation of stochastic processes. The (two-sided) PSD based on DOST coefficients is defined as (Cui and Hong 2020),

$$S_{DS}(p,q) = x_{DS}(p,q)x_{DS}^*(p,q) \qquad (13)$$

The (two-sided) PSD defined based on DHWT coefficients is defined as (Spanos et al. 2005),

$$S_{DH}(b,q) = x_{DH}(b,q)x_{DH}^*(b,q) \qquad (14)$$

It can be shown that the total energy of signals in the time domain equals that in the transformed domain for DOST and DHWT,

$$\begin{aligned}\sum_k |x(t_k)|^2 &= (1/N)\sum_{\text{all } p,q} S_{DS}(p,q) \\ &= (1/N)\sum_{\text{all } b,q} S_{DH}(b,q)\end{aligned} \qquad (15)$$

Again, it must be emphasized that the energy preservation shown in Eq. (15) is adequate for DHWT only if the DHWT coefficients are obtained through the implemented algorithm shown in Figure 3. In other words, such an implementation ensures perfect reconstruction and energy preservation.

An illustration of the PSD functions of the record shown in Figure 1a based on DOST and DHWT is depicted in Figure 5 in time-frequency space and time-scale space, respectively.

## 4. EDGE EFFECTS IN SIMULATION

The use of DOST to simulate the nonstationary Gaussian processes was proposed by Cui and Hong (2020) by randomizing the phase of the DOST coefficients,

$$x_s(t_k) = \sum_{\text{all } p,q} \sqrt{S_{DS}(p,q;\beta)} \times D_{[\beta]}^*(t_k;p,q)e^{i\phi(p,q)} \qquad (16)$$

where $\phi(p, q)$ is the phase. By randomizing the phase of DHWT coefficients, the nonstationary Gaussian process could be simulated by (Spanos et al. 2005),

$$x_s(t_k) = \sum_{\text{all } b,q} \sqrt{S_{DH}(b,q)}\psi_{DH}(t_k)e^{i\phi(b,q)} \qquad (17)$$

where $\phi(b, q)$ is the phase.

For DOST, the direct use of Eq. (16) in the time domain or based on the algorithm in Figure 3 leads to the same results. However, for DHWT, Eq. (17) should not be directly used to generate samples to avoid energy distortion in sampled records (Liu et al. 2022). To ensure energy preservation, the simulation should be carried out in the frequency domain (i.e., the algorithm shown in Figure 3). Moreover, FFT could be adopted to gain computational efficiency.

For example, by considering the PSD shown in Figure 5a as the target, we sample 1000 samples by using Eq. (16), with a typical sample shown in Figure 6a. Although the total energy is preserved in the simulated records as shown in Hong and Cui (2020), it can be observed that some of the energy is shifted to the edges of the records as can be observed from the mean of the standard deviation $\sigma(t)$ of the amplitude of the simulated 1000 records shown in Figure 6b, where $\sigma^2(t)$

for a sampled record is evaluated using a moving window with 2-second width. This observed edge effect is not very significant. However, our experience indicates that it can be important for signals where a large energy difference between the two edges for the target PSD function exists.

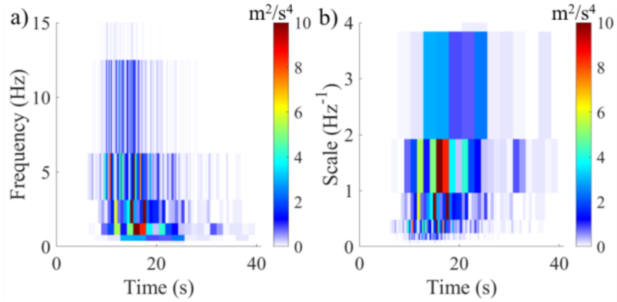


*Figure 5: The PSDs of the ground motion record shown in Figure 1a based on DOST or DHWT in a) time-frequency space b) time-scale space.*

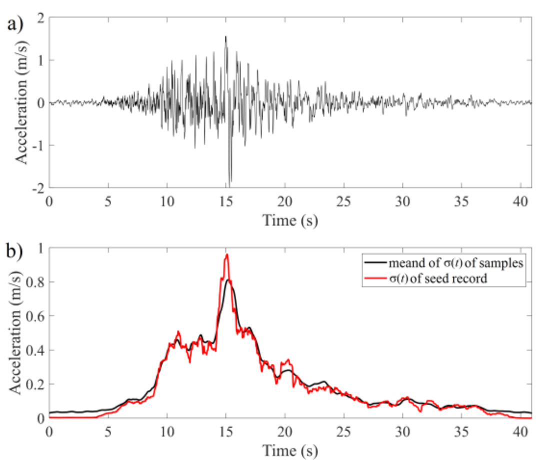


*Figure 6: a) a simulated sample; b) the mean of σ(t) of simulated samples compared to that of record shown in Figure 1a.*

In cases where very accurate matching of the target σ(*t*) is required for the record simulation by using Eq. (16), an iterative correction procedure proposed in the following could be used. This correction procedure is explained in the following by using an example. More specifically, consider the target σ(*t*), $\sigma_T(t)$, equals that shown in Figure 6b, which is calculated from the seed record shown in Figure 1a. The steps of the correction procedure are:

1) Simulate $m_s$ samples, denoted as $x_{S,j}(t)$, $j = 1,\ldots,m_s$, based on Eq. (16) with $S_{DS}(p,q;\beta)$ equal to its target PSD;
2) Calculate the time-varying variance from the set of sampled records $x_{S,j}(t)$, denoted as $\sigma^2_s(t)$, and the relative error ε,

$$\varepsilon = \sum\left(\sigma_T(t_k) - \sigma_s(t_k)\right)^2 / \sum \sigma_T(t_k)^2 \quad (18)$$

3) If ε is less than the specified tolerance $\varepsilon_T$, stop the iteration. Otherwise, replace $x_{S,j}(t)$ by $x_{S,j}(t)\times\left(\sigma_T(t)/\sigma_s(t)\right)$, and calculate the phase of the *j*-th record $x_{S,j}(t)$, $\phi_j(p,q)$ or $\phi_j(b,q)$, where $j = 1,\ldots, m_s$;
4) Calculate $x_{S,j}(t)$, $j = 1,\ldots, m_s$, by using Eq. (16) with the target PSD and the updated phased $\phi_j(p,q)$ or $\phi_j(b,q)$. Repeat Steps 2) and 3) until convergency is reached.

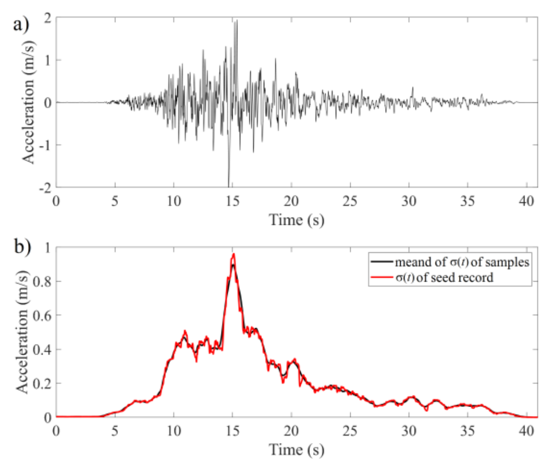


*Figure 7: a) a simulated sample based on the proposed algorithm; b) the mean of σ(t) of simulated samples compared to that of the record shown in Figure 1a.*

By using the proposed algorithm with DOST (i.e., Eq. (16)) and setting the $\varepsilon_T$ and $m_s$ equal 1E-5 and 1000, a simulated sample is shown in Figure 7a. The mean of σ(*t*) calculated from the 1000 sampled records is shown in Figure 7b, indicating an improved matching to $\sigma_T(t)$ as compared to that shown in Figure 6b. Since the PSD of each sample record is practically identical to the target PSD shown in Figure 5, its statistics are not shown.

## 5. CONCLUSIONS

Two efficient transforms are reviewed: discrete harmonic wavelet transform (DHWT) and discrete orthonormal S-transform (DOST), and detailed comparisons of these two transforms are presented. The comparison is focused on 1) their mathematical derivations of basis functions; 2) computational implementation; 3) representation in time-frequency or time-scale space. The main observations concluded:

1) The basis functions for DOST and DHWT are both derived by wrapping the Fourier representation over a band frequency. However, the basis function for DOST is derived based on DFT while that for DHWT is derived based on CFT.
2) The basis functions for DOST are orthonormal for the finite duration of the considered digitized signal. This is not the case for DHWT; where the orthonormal condition is true by considering the entire real axis (i.e., duration from negative infinite to positive infinite);
3) The computational implementation of both DOST and DHWT are the same except an additional phase shift is considered for DOST to ensure the absolutely referenced phase;
4) DHWT provides a representation in the time-scale space while DOST gives a representation in the time-frequency space. Both adopt the octave sampling scheme. There exists a mapping between these two spaces.

The use of DOST and DHWT to simulate nonstationary signals (e.g., seismic ground motions) is very simple. The possible edge effect due to the coarse resolution (as compared to continuous transform) could be ameliorated by using the iterative algorithm in the present study.

## 6. ACKNOWLEDGEMENT

We gratefully acknowledge the financial support received from the Harbin Institute of Technology, Western University, and the Natural Sciences and Engineering Research Council of Canada (RGPIN-2019-05160, for WXZ; RGPIN-2016-04814, for HPH).

## 7. REFERENCES

Bracewell, R. N., (1986). The Fourier transform and its applications. New York: McGraw-Hill.

Cui, X.Z., and Hong, H.P. (2020). Use of discrete orthonormal S transform to simulate earthquake ground motions. Bulletin of the Seismological Society of America, 110(2), 565-575.

Daubechies, I. (1992). Ten lectures on wavelets. Society for industrial and applied mathematics. Pennsylvania

Hong, H.P., and Cui, X.Z. (2020). Time–frequency spectral representation models to simulate nonstationary processes and their use to generate ground motions. Journal of Engineering Mechanics, 146(9), 04020106.

Hong, H. P., Cui, X. Z., and Xiao, M. Y. (2021). Modelling and simulating thunderstorm/ downburst winds using S-transform and discrete orthonormal S-transform. Journal of Wind Engineering and Industrial Aerodynamics, 212, 104598.

Liu, Y.X., Cui, X.Z. and Hong, H.P. (2022). On the suitability of using discrete and continuous harmonic wavelets for analyzing, modeling, and simulating uni- and multivariate nonstationary non-Gaussian processes. Submitted for publication.

Newland, D.E. (1993). Harmonic wavelet analysis. Proceedings of the Royal Society A Mathematical Physical & Engineering Sciences

Newland, D.E. (1994). Wavelet analysis of vibration, part 2: Wavelet maps, Journal of Vibration and Acoustics, Trans. ASME. Vol. 116, 417-425.

Spanos PD, Tezcan J, Tratskas P. (2005) Stochastic processes evolutionary spectrum estimation via harmonic wavelets. Computer Methods in Applied Mechanics and Engineering; 194(12-16): 1367-1383.

Spanos PD, Failla G. (2004) Evolutionary spectra estimation using wavelets. Journal of Engineering Mechanics; 130(8): 952-960.

Stockwell, R.G. (2007). A basis for efficient representation of the S-transform. Digital Signal Processing, 17(1), 371-393.

Stockwell, R.G., Mansinha, L., and Lowe, R. P. (1996). Localization of the complex spectrum: the S transform. IEEE transactions on signal processing, 44(4), 998-1001.

Wang, Y., and Orchard, J. (2009). Fast discrete orthonormal Stockwell transform. SIAM Journal on Scientific Computing, 31(5), 4000-4012.